Nanoscale

Negative Differential Resistance Observed on the Charge Density Wave of a Transition Metal Dichalcogenide

Journal:	*Nanoscale*
Manuscript ID	NR-ART-09-2019-007857.R2
Article Type:	Paper
Date Submitted by the Author:	06-Nov-2019
Complete List of Authors:	Luican-Meyer, Adina; Argonne National Laboratory, Center for Nanoscale Materials Zhang, Yuan; Argonne National Laboratory, Center for Nanoscale Materials DiLullo, Andrew; Argonne National Laboratory, Center for Nanoscale Materials Li, Yang; Ohio University, Physics and Astronomy Dept. Fisher, Brandon; Argonne National Laboratory, Center for Nanoscale Materials Ulloa, Sergio ; O, Sergio Ulloa; Sergio Ulloa Hla, Saw-Wai; Ohio University, Physics and Astronomy Dept.; Argonne National Laboratory, Center for Nanoscale Materials

Negative Differential Resistance Observed on the Charge Density Wave of a Transition Metal Dichalcogenide

Adina Luican-Mayer[1+3], Yuan Zhang[1+], Andrew DiLullo[1], Yang Li[1,2], Brandon Fisher[1], Sergio E. Ulloa[2], and Saw-Wai Hla[1,2,*]*

[1]Center for Nanoscale Materials, Argonne National Laboratory, 9700 South Cass Ave., Argonne, Illinois 60439, United States.

[2]Nanoscale and Quantum Phenomena Institute, and Department of Physics & Astronomy, Ohio University, Athens, Ohio 45701, United States.

[3]Department of Physics, University of Ottawa, 150 Louis Pasteur Private, Ottawa, Canada.

KEYWORDS: Charge Density Wave, Scanning Tunneling Microscopy, Negative Differential Resistance, Transition Metal Dichalcogenides

Corresponding Author

* Corresponding authors email: hla@ohio.edu ; luican-mayer@uottaw.ca

Present Addresses

+Current Address: Department of Physics, Old Dominion University, 4600 Elkhorn Ave, Norfolk, VA 23529, USA.

Abstract:

Charge density waves and negative differential resistance are seemingly unconnected physical phenomena. The former is an ordered quantum fluid of electrons, intensely investigated for its relation with superconductivity, while the latter receives much attention for its potential applications in electronics. Here we show that these two phenomena can not only coexist but also that the localized electronic states of the charge density wave are essential to induce negative differential resistance in a transition metal dichalcogenide, 1T-TaS_2. Using scanning tunneling microscopy and spectroscopy, we report the observation of negative differential resistance in the commensurate charge density wave state of 1T-TaS_2. The observed phenomenon is explained by the interplay of interlayer and intra-layer tunneling with the participation of the atomically localized states of the charge density wave maxima and minima. We demonstrate that lattice defects can locally affect the coupling between the layers and are therefore a mechanism to realize NDR in these materials.

Introduction

Low dimensional materials such as transition metal dichalcogenides (TMDCs) have stimulated an intense interest due to the wide range of physical properties they exhibit [1,2,3], including novel quantum phenomena in 2D monolayers[4], 2D multi-stack heterostructures[5], as well as their potential applications[6]. Among these materials, 1T-TaS_2 has attracted considerable attention as a result of its rich phase diagram[1], which includes the formation of charge density waves (CDW)[7,8,9,10,11,12]. In 1T-TaS_2, tantalum (Ta) atoms have octahedral coordination with the sulphur (S) atoms (Figure 1a) and a commensurate CDW phase develops at low temperatures. This commensurate CDW phase exhibits a complex lattice distortion[13] where the Ta atoms are arranged in groups of 13 atoms, a configuration typically referred to as the 'Star-of-David' structure (Figure 1b). Experimental and theoretical work demonstrated that the relative orientation of the orbitals within the 2D sheets of 1T-TaS_2 with respect to those in successive layers can significantly modify the overlapping integrals across the material, leading to changes in the electronic properties of the system[14,15]. As a result, it was proposed that device applications could exploit such orbital order in the CDW phase of 1T-TaS_2.

Here we report the experimental observation of yet another intriguing phenomenon arising from the intricacies of the orbital order - a negative differential resistance (NDR) in 1T-TaS_2. We further investigate the local electronic properties with tunneling spectroscopy and spectroscopic mapping, which provides unprecedented information at the atomic scale on CDW and the appearance of negative differential resistance. We present a model for understanding this phenomenon based on a balance between inter- and intralayer coupling of electronic

states that is sensitive to effects such as local stacking order, and the presence of defects or domain boundaries.

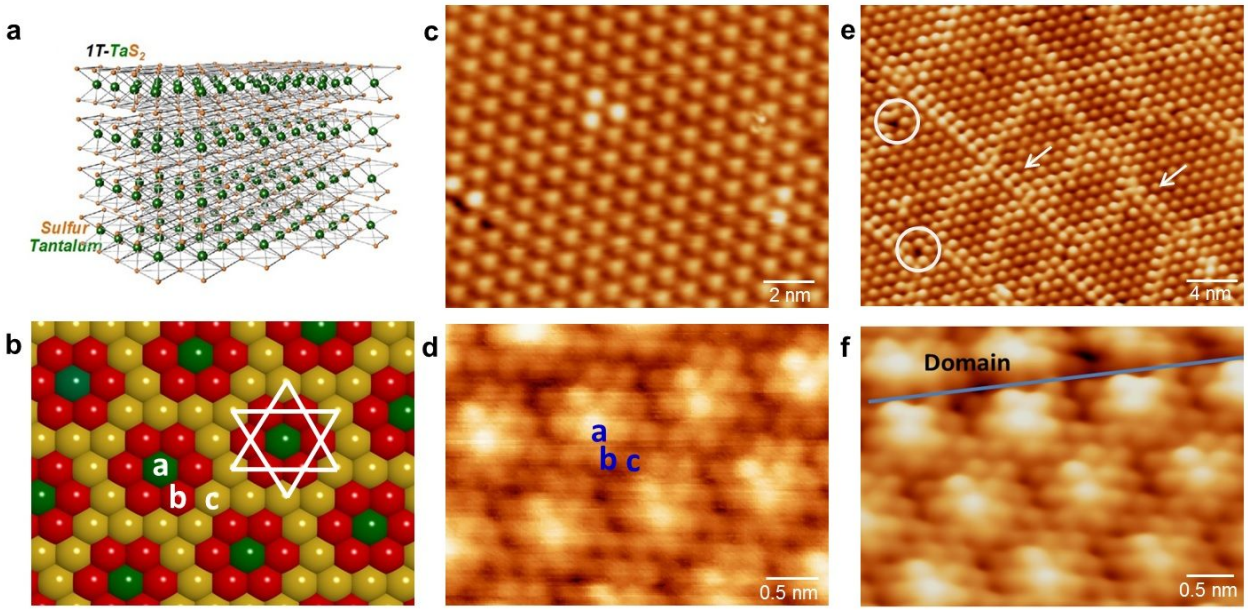

Figure 1. *1T-TaS_2 crystal structure.* ***a****, A 3-D structural model of 1T-TaS_2 where S-Ta-S sandwiches are separated by vdW gaps.* ***b****, A ball model showing 3 types of atoms in the Ta layer labelled as a, b, and c. The star-of-David structure is indicated.* ***c****, Large area STM image showing CDW formation in 1T-TaS_2 [Imaging parameters: V_t = 1V, I_t = 1 nA].* ***d****, STM image showing Ta atoms in the CDW [Imaging parameters: V_t = 1V, I_t = 1 nA].* ***e****, Formation of textured CDW faces and domains after applying voltage pulses and mechanical contact with the STM tip [Imaging parameters: V_t = 1V, I_t = 3 nA]. The circles indicate defects while the arrows indicate domain boundaries.* ***f****, Atomic scale STM image showing a CDW domain boundary after voltage pulsed induced manipulation with the STM tip [Imaging parameters: V_t = 1V, I_t = 1 nA].*

The experiments were conducted on the surface of a freshly cleaved 1T-TaS_2 in ultrahigh vacuum environment with a base pressure below 10^{-10} Torr and using a Createc low temperature scanning tunneling microscope (STM) system. For measurements, a freshly cleaved TaS_2 crystal was introduced to the UHV chamber and then subsequently cooled down to 11 K for STM imaging and tunneling spectroscopy measurements. dI/dV tunneling

spectroscopy and spectroscopic maps were acquired with a lock-in amplifier with a voltage modulation of 5 to 20 meV and a frequency range of 750 Hz to 1 kHz. STM manipulations were performed by applying voltage pulses up to 4 V and by extending the 'z' piezo to achieve mechanical contact with the sample surface.

Results and discussion

Figure 1c presents an STM topographic image acquired on the surface of 1T-TaS_2, where the observed periodic pattern is the well-known $\sqrt{13} \times \sqrt{13}$ structure of a commensurate CDW phase. A highly resolved STM topograph of 1T-TaS_2 (Figure 1d) reveals the detailed atomic structure of the CDW. Although the chalcogen atoms are located at the top surface layer in TMDCs, STM images near the Fermi level are generally contributed by the d_z orbitals of the transition metal atoms pointing normal to the surface[16]. This assignment is in agreement with density of states calculations reported in the literature[14,28,33]. Figure 1d shows the periodic distortion forming the Star-of-David structure, within which one can distinguish 3 types of Ta atoms, a, b, and c, by their dissimilar intensities. The 'a' atoms are located at the CDW top sites with each 'a' atom surrounded by six 'b' atoms while the 'c' atoms are located at the valleys of the CDW, i.e. the CDW minima. The observed CDW lattice is commensurate and rotated ~13° from the underlying Ta lattice.

The CDW structure of 1T-TaS_2 is found to occasionally deviate from the ideal one described above. In fact, it can be deliberately altered by applying voltage pulses with an STM tip[17]. Figure

1e shows a topographic map of a 1T-TaS_2 surface area decorated with domain networks after manipulation with the STM tip by applying 2.5 V voltage pulses. Such tip-induced manipulation

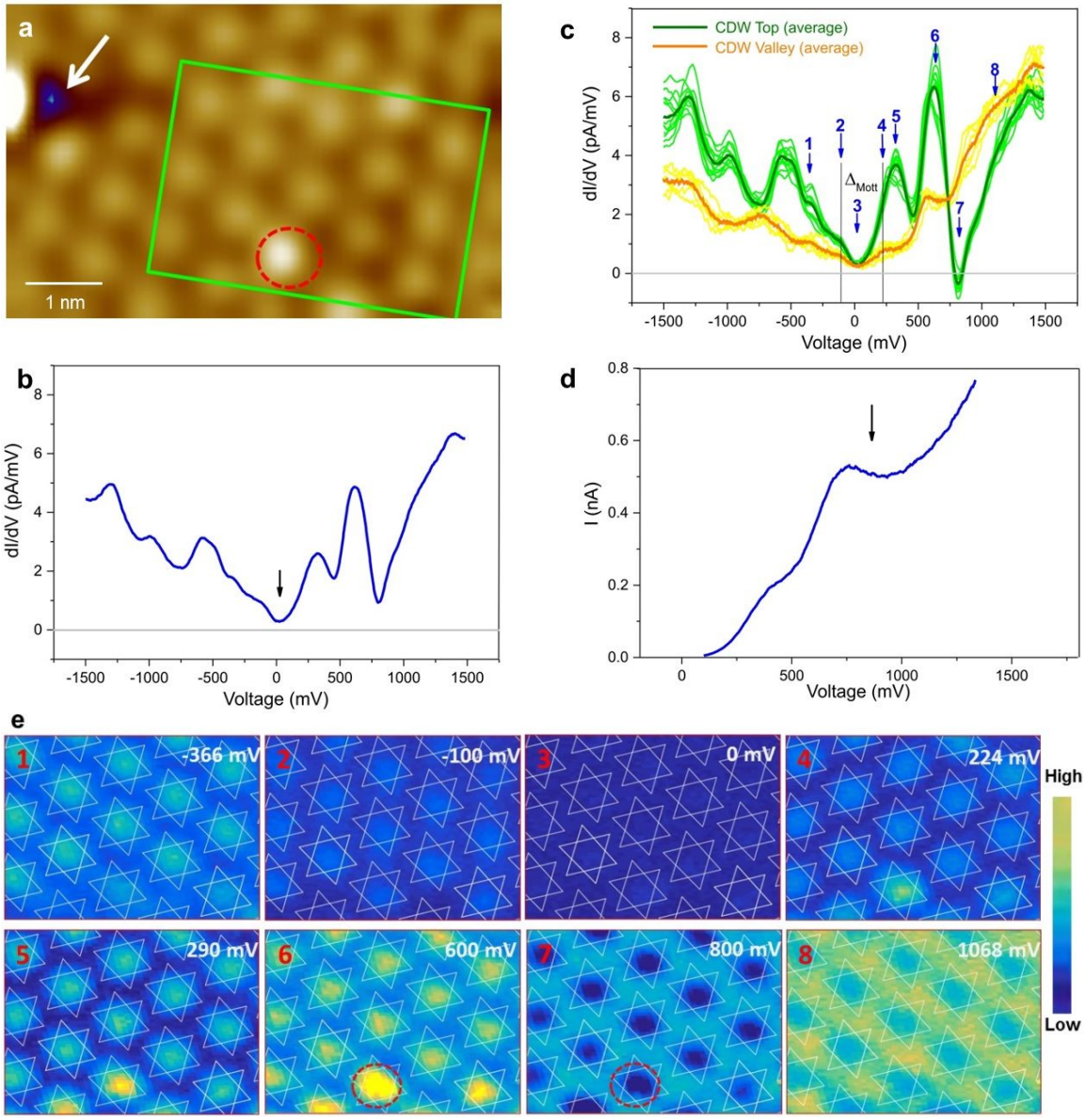

Figure 2. *NDR region of 1T-TaS_2.* ***a****, STM image of 1T-TaS_2 region after tip sample mechanical contact at left (indicated with white arrow). The green rectangular region is where the spectroscopy data are acquired [Imaging parameters: V_t = 1V, I_t = 1 nA].* ***b****, dI/dV spectroscopy data averaged over all three atom sites of 1T-TaS_2. The Mott gap is indicated with an arrow.* ***c****, dI/dV spectroscopic data corresponding to CDW top (light green) and valley (yellow) sites. The average dI/dV data of the CDW top and valley are shown as green and orange plots.* ***d****, Average I-V data of CDW top sites. The arrow indicates the NDR region.* ***e****, dI/dV spectroscopic maps corresponding to bias values labelled as 1 to 8 in 'c'. The Star of David structure is overlaid for guidance. Dashed circles indicate a local defect. The maps 1 and 5 show the highest intensities*

at the CDW top sites while the maps 2 and 4 belong to the lower and upper Hubbard bands respectively. Map 3 is located at the Fermi level within the Mott gap, where no apparent features are observed. The map 7 shows the NDR appear as darker regions at the centres of the Star of David structures. Map 8 reveals an increase in intensity at the C atom locations next to the NDR regions.

results in shifting of the CDW positions, so that adjacent CDW domains become separated by clear boundaries (Figure 1e, and 1f). The voltage pulse manipulation can also alter the stacking order between adjacent layers[18,19] (Supplementary Figure S1), and it can cause a strong modulation of the Mott insulating state[20]. Local defects can also be created using a controlled tip-sample contact[21] (Figure 1e) and such defects can cause shifting of the vertical stacking order of the 1T-TaS_2 layers as well.

Negative differential resistance (NDR) can be attributed, in a broad sense, to band level alignment of electronic features in materials producing an effective resonant tunneling geometry. NDR was observed in different systems such as molecules adsorbed on semiconductors[22] or metal substrates[23]. NDR can also occur in resonant tunneling between localized electronic states of the STM tip and the surface[24]. In bilayer graphene, NDR originates from the two near-gap van Hove singularities that are strongly localized in the two sub-lattices in different graphene layers[25].

Here, we report the observation of NDR in a new material system, 1T-TaS_2, with a charge density wave structure. Figure 2a presents the STM topographic image of a 1T-TaS_2 surface area including the region were we investigated the appearance of NDR, marked by a green rectangle. The average tunneling spectroscopy data collected from the region in Figure 2a

shows similar features to those observed in other STM measurements[17,18,26,27], with a Mott gap of ~250 meV at the Fermi level (Figure 2b)[28,29,30,31]. In agreement with previous reports, the density of states in the CDW phase exhibits features that originate in subbands of the 5d orbitals. We note that the precise energy position and width of these subbands is strongly dependent on the local stacking[14,27,32,33], and likely responsible for the slight sample-to-sample variations in measured STS spectra. Interestingly, clear differences emerge when the spectra are selectively collected at the location of the 'a' and 'c' atoms (Figure 2c) corresponding to the CDW top and valley sites, i.e. the CDW maximum and minimum locations, respectively (Figure 1b and 1d). Except in the vicinity of the Fermi level, both the intensity and energy positions of the peaks in the dI/dV spectra appear completely different for the top and valley sites. The CDW top sites are dominant for the occupied states as well as near the Fermi level, while the valley sites take the lead for the unoccupied states above 730 mV. Importantly, we find that the dI/dV on top sites exhibits NDR at ~800 meV (Figure 2c). Accordingly, this is also reflected in the average I-V spectroscopy data measured across the CDW top sites (Figure 2d). We note that the dI/dV spectra of 'b' sites are essentially given by the average dI/dV data between the 'a' and 'c' sites (Supplementary Figure S4), with most pronounced features being localized at the 'a' and 'c' atoms within the Star-of-David structure.

The spatial variations of the electronic structure are directly visualized by means of dI/dV spectroscopic mapping with atomic scale resolution, allowing us to gain further insight into the relationship between the CDW and NDR. A total of 3000 dI/dV spectroscopic maps were acquired in the bias range -1500 mV and +1499 mV, with 1 mV interval (see the STS map movie

in Supplemental Information). This measurement provides unprecedented information on the electronic structure modulations and the evolution of NDR within the Star-of-David structure at the atomic scale. Figure 2e presents a sequence of dI/dV spectroscopic maps acquired at biases marked as 1 to 8 in Figure 2c. The maps 1 and 5 show the highest intensities at the CDW top sites at the centre of the Star-of-David structure. Maps 2 and 4 belong to the lower and upper Hubbard bands respectively (Figure 2c), and display faint intensity at the CDW top sites. No apparent features are observed at the bottom of the Mott gap located around the Fermi level (map 3). These tunneling spectroscopic maps confirm that the vicinity of the Mott gap region is mainly contributed by the CDW top sites, i.e. by 'a' atoms.

At ~800 mV the intensity in the dI/dV spectra of the CDW top sites decreases below zero, while that belonging to the CDW valley sites increases. Accordingly, the I-V plots measured at the CDW top sites shown in Figure 2e reveal NDR at ~800 mV (map 7). The dI/dV spectroscopic maps highlight the atomically localized nature of the observed NDR. For instance, map 6 at 600 mV shows a high intensity at the CDW top sites. However, map 7 at 800 mV completely reverses the intensity and the CDW top sites now appear darker. Thus, the observed NDR is strongly localized at the CDW top sites. At higher positive voltages, larger than the one where NDR is observed, the CDW valley continues to dominate the dI/dV signal as evident in the spectroscopic map 8 taken at 1036 mV.

We now turn to interpreting the mechanism of the observed of NRD in this system. Firstly, in our experiments, the involvement of the STM tip states in the NDR process can be ruled out

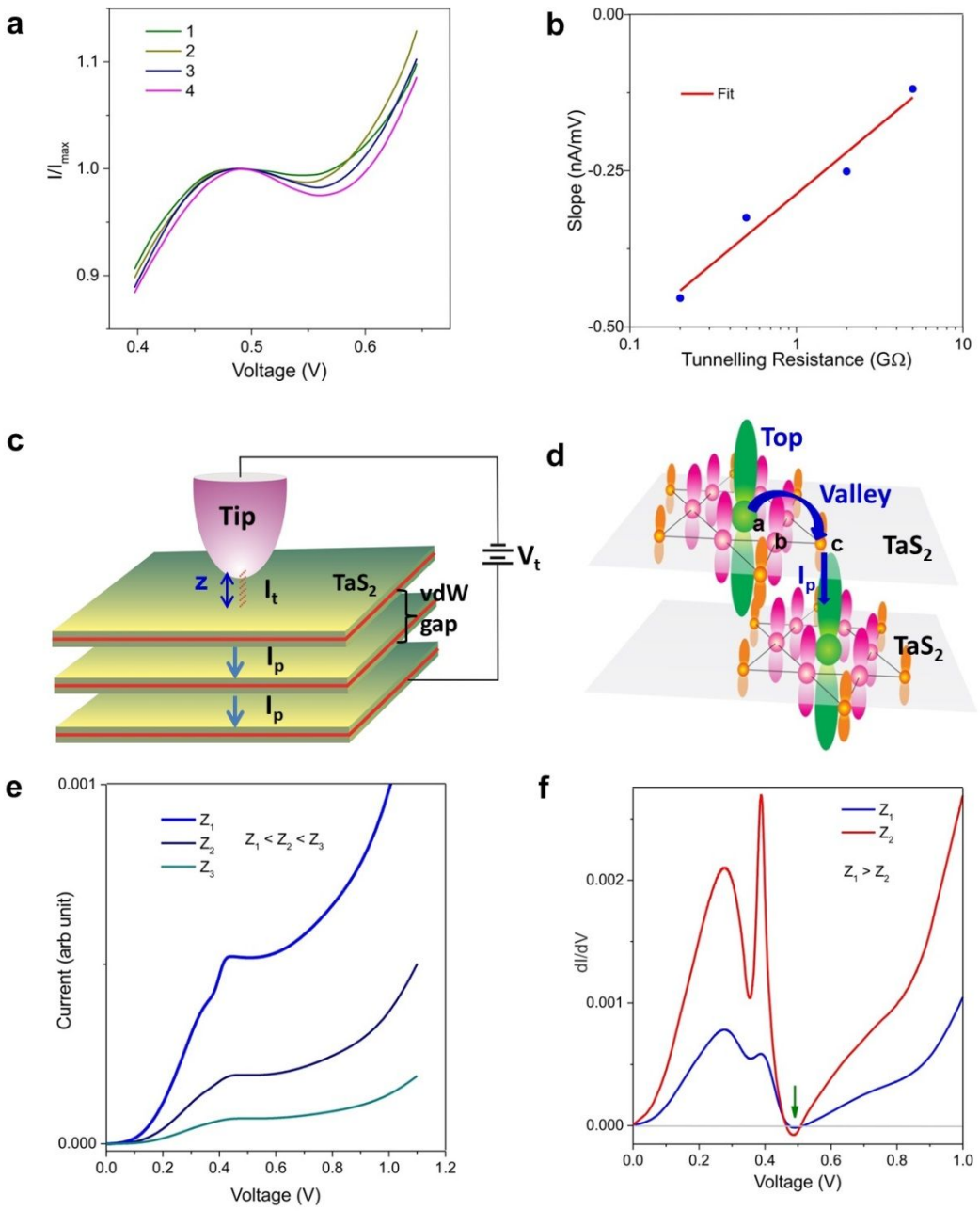

Figure 3. *NDR mechanism.* ***a****, I-V data measured at a centre of a CDW top site with varying tip heights. Tunneling resistance, R_t = 5 GΩ (1), 2 GΩ (2), 0.5 GΩ (3), and 0.2 GΩ (4). The initial set tunneling currents for curves 1,2,3 and 4, are 0.2 nA, 0.5 nA, 1 nA, and 2 nA, respectively, and the initial set bias is +1V for all measurements.* ***b****, The slope, ΔI/ΔV, as a function of tunneling resistance.* ***c****, A drawing depicting STM tip-sample geometry of the experiment where the tunneling current (I_t) passes to the different layers of 1T-TaS_2 as I_p.* ***d****, A schematic representation of the current flows from the CDW top (a atom) to valley (c atom) then to adjacent layer below.* ***e****, Simulated dI/dV for two different tip heights show stronger NDR (green arrow) when the tip is closer to the surface.* ***f****, Simulated I-V plots for different tip heights.*

because the dI/dV spectra acquired at different locations with the same tip do not show such a tip state (map 7). Instead, the two localized states essential for the NDR mechanism are apparent in the dI/dV spectra (Figure 2c) as well as in the dI/dV spectroscopic maps (Figure 2e). The NDR in this system is always observed on the CDW top sites, as the differential conductance dips below zero, while the electronic structure of the valley sites is consistently larger.

To gain further insight into the NDR mechanism, I-V spectroscopy measurements were performed with different tip heights using a fixed bias of 1V with varying tunneling currents (Figure 3a), where the lower the tunneling resistance (R_t), the closer the tip is to the surface. By changing R_t from 5 GΩ to 0.2 GΩ, the negative slope of the I-V curves becomes more noticeable. Accordingly, the corresponding dI/dV spectra exhibit a clear NDR dip behavior (Supplementary Information S5). Figure 3b shows the measured negative slopes (ΔI/ΔV) as a function of R_t, which reveals that by approaching tip or reducing R_t, the NDR becomes more pronounced. This measurement was performed on the CDW top site '3' in Figure 4a.

We note that for a C_{60} double layer formed on a Au(111) surface[22], the tunneling voltage-dependent barrier height was found responsible for the presence of NDR. In that case, a larger tip-height, therefore a higher R_t, results in a stronger NDR. In the case of CDW in 1T-TaS_2, however, we observe an opposite trend, where a reduced tip-height enhances the NDR (Figure 3a and 3b), so that the bias dependent tunneling barrier can be ruled out as the origin. Based on the tip-sample geometry of our measurements (Figure 3c), the tunneling current (I_t) arriving

at the top surface layer of 1T-TaS_2 is required to pass through the adjacent layers underneath. The passing current, I_p, strongly depends on the vertical coupling between adjacent 1T-TaS_2 layers, as well as in lateral paths, as shown schematically in Figure 3d.

To model the effects of inter- and intralayer coupling, we consider a typical expression for the tunneling current given in terms of DOS and the tunneling probability of electrons from the tip as,

$$I = \int_0^V \eta(E,z)T(E,V,z)dE \quad . \quad (1)$$

In this expression, intralayer coupling is accounted for in the local DOS, $\eta(E,z)$, having features with effective widths that depend on the tip distance from the surface, z. The interlayer coupling is reflected in the tunneling probability, *T*, having a characteristic WKB form that depends on the work function ϕ, and considers tilting of the vacuum barrier separating the tip and sample, $T = e^{-z\,C\sqrt{\phi - E + V/2}}$. Here, C is a constant that depends on electron mass and natural constants ($\simeq 1.15\ \text{Å}^{-1}eV^{-1/2}$). For simplicity the tip is assumed to be featureless in this region. The differential conductance dI/dV can then be written as:

$$\frac{dI}{dV} = \eta(E,z)T(E,V,z)|_{E=V} + \int_0^V \eta(E,z)\frac{\partial T(E,V,z)}{\partial V}dE \ . \quad (2)$$

For the theoretical analyses, the DOS is modeled with five Gaussians to mimic data for bias in the [0,1]Volt region in the images of Figure 4b. Approaching the tip to the surface is assumed to narrow the width of the Gaussian at 0.4V by a factor f. Here, f = 0.5, 1, and 1.2 are used for Z_1,

Z_2 and Z_3 tip heights in Figure 3, respectively. Figure 3e shows the results for two different tip heights, $Z_1 < Z_2$. Although the system exhibits NDR for both tip-heights, the closer tip height Z_1

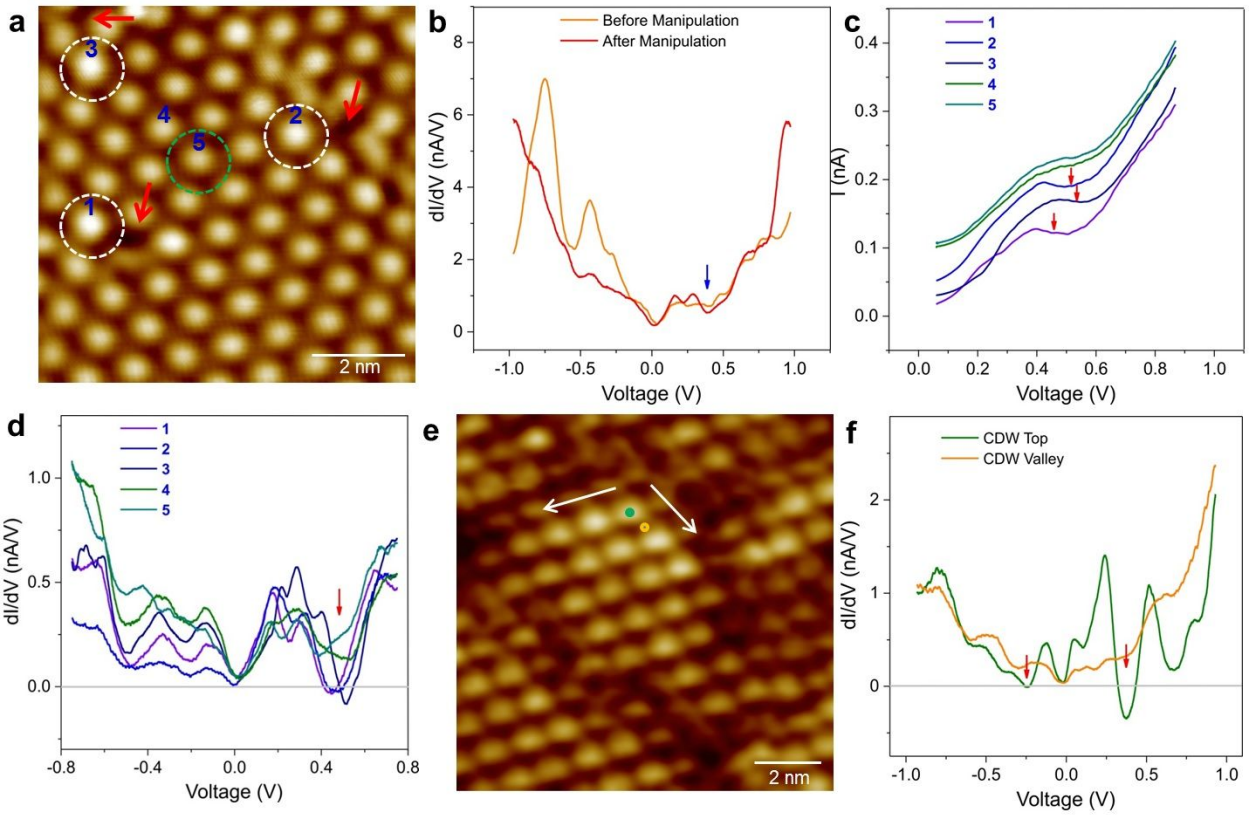

Figure 4. *NDR and surface defects.* ***a****, STM image shows three point defects created at the locations indicated with red arrows on 1T-TaS_2. Bright CDW top sites appear next to the defect sites (shown with white ovals) [Imaging parameters: V_t = 1V, I_t = 0.2 nA].* ***b****, dI/dV spectra of the CDW top site marked with a green oval in 'a' reveal the electronic structural changes before and after manipulation. The arrow indicates a deeper dip after the manipulation.* ***c****, The I-V spectra corresponding to CDW top sites 1 to 5 in 'a'. The spectra acquired at the sites, 1, 2, and 3, show NDR, which are indicated with the arrows.* ***d****, The dI/dV spectra acquired on the 5 CDW top sites, 1,2,3,4, and 5 in 'a'. Here the spectra 1,2, and 3 show NDR (indicated with a red arrow).* ***e****, STM image after voltage pulse manipulation of 1T-TaS_2 surface shows formation of domain networks (shown with arrows) [Imaging parameters: V_t = -1V, I_t = 0.63 nA].* ***f****, dI/dV spectra measured at the CDW top (green) and valley (orange) locations shown with dots in 'e'. The CDW top spectrum reveals NDR at both occupied and unoccupied states (indicated with red arrows).*

induces a stronger decoupling between the CDW top and valley sites, thereby enhancing the apparent DOS features, while the corresponding NDR values increase by a factor of ~5. Such

effect can also be observed in the I-V characteristics shown in Figure 3f, where reducing the tip-height ($Z_1 < Z_2 < Z_3$) increases the current as well as the NDR effect. One can imagine that as the tip approaches the intralayer coupling between the CDW top and valley sites is likely reduced, akin to an effective gating by the tip, which enhances the spatial localization of the Star-of-David sites, and then produces sharper features (smaller bandwidths) in the highly-structured local density of states $\eta(E,z)$. To understand the phenomena responsible for changes in the interlayer coupling, we note that naturally occurring crystal defects or defects induced by tip manipulation can not only shift CDW lattice laterally but can also reduce the vertical coupling, i.e. orbital hybridization, between adjacent layers[31,32].

We present experimental evidence demonstrating how defects on the surface of 1T-TaS_2 can affect the realization of conditions necessary for NDR, likely by tuning the interlayer and intralayer couplings as discuss before. To that end, we focus on defects that are tip-induced and explore their electronic properties. Figure 4a shows three defect sites formed by STM tip manipulation (indicated by red arrows in Figure 4a and Supplementary Figure S2) where the CDW top sites next to the structural defects appear brighter (marked with white ovals). Creation of such defects alters the local electronic structural environment, as evident in the dI/dV spectra (Figure 4b) acquired on a CDW top site shown with a green oval in Figure 4a. Here, the unoccupied states appear more pronounced after the manipulation, with sharper Hubbard band edges and a deeper dip (here at ~0.4V), while the occupied states become broader. Remarkably, the negative differential resistance (NDR) signals are observed when I-V spectroscopic data are measured by positioning the STM tip above the three bright CDW top

sites 1, 2, and 3 in Figure 4a while similar I-V curves on neighboring CDW top sites 4, and 5 show no NDR and only a slight decrease in the current occurs (Figure 4c). Accordingly, the differential conductance (dI/dV signal) of the sites 1, 2, and 3 drops below the zero level (Figure 4d). The NDR can also be observed at negative biases after STM tip-induced manipulation. Figure 4e presents a 1T-TaS_2 surface area where a domain network develops after an STM tip-induced manipulation. The dI/dV tunneling spectroscopy measured above CDW top and valley sites (green and yellow dot locations respectively in Figure 4e) are presented in Figure 4f. Here, the dI/dV spectrum of the CDW top site reveals NDRs at both positive (+0.37 V) and negative (-0.25V) biases. We note that the precise energy where the NDR is present depends on the local energies of the 5d orbital subbands, which are sensitive to local stacking and interlayer coupling, and therefore can differ across the sample. Consistent with the data presented in Figure 2, in contrast to the CDW top site, the NDR is absent in the spectrum of the CDW valley sites. These results suggest that the presence of crystal defects can strongly affect the local orbital order and sensitivity to the gating effect of the approaching STM tip. A closer look at Figure 2a reveals that the extended area exhibiting NRD is in the vicinity of several defects that are likely responsible for balancing the interlayer and intralayer coupling such that NDR is observed.

Conclusions

In summary, the observation of NDR in the charge density wave phase of 1T-TaS_2 is facilitated by the localized states between the CDW top and valley sites and the local changes in the vertical coupling between the orbitals in adjacent layers induced by STM tip manipulations.

Since the localized states here are centered at the CDW top and valley sites, the charge density structure in 1T-TaS_2 is paramount to induce the observed NDR. Moreover, the out-of-plane stacking can significantly affect the interlayer coupling in this material, which in turn strongly influences the tunneling processes. As demonstrated here, local regions and defects formed by voltage pulses can disturb the interlayer coupling, as in the regions depicted by Figure 4, or in extended regions, as in Figure 2. Although we have not explored naturally occurring defects on TaS_2 in this work, one can speculate that if appropriate conditions for intra and interlayer coupling are provided, then not only defects, but also other stimulus such as high pressure or intercalants would induce NDR. The observation of NDR on CDW phase opens exciting potential applications of two-dimensional materials for electronic and nanoscale devices.

Conflicts of interest

There are no conflicts to declare.

Author Contributions

S.W.H. and A.L.M. conceived and designed the experiments: A.L.M., Y.Z., A.D. and Y.L. performed the STM experiments; B.F. provided the technical support for the experiments, S.E.U performed theoretical analyses, A.L.M., Y.Z., A.D., Y.L., and S.W.H. analyzed the experimental data. All the authors discussed the results and commented on the manuscript. +These authors contributed equally.

Acknowledgements

This work was performed at the Center for Nanoscale Materials, a U.S. Department of Energy Office of Science User Facility, and supported by the U.S. Department of Energy, Office of Science, under Contract No. DE-AC02-06CH11357. Y.L. and S.W.H. acknowledge the support from U.S. Department of Energy, Office of Science, Office of Basic Energy Sciences grant No. DE-FG02-02ER46012 for a part of STM measurements. We acknowledge discussions with Pierre Darancet. S.E.U. acknowledges support from NSF grant DMR 1508325. A.L.M. acknowledges funding from the National Sciences and Engineering Research Council (NSERC) Discovery Grant RGPIN-2016-06717. Part of the discussions between A.L.M. and S.E.U. about the interpretation of the data was performed at the Aspen Center for Physics which is supported by NSF grant PHY-1607611.

References

[1] J.A. Wilson, and A.D. Yoffe, The Transition Metal Dichalcogenides Discussion and Interpretation of the Observed Optical, Electrical and Structural Properties, *Adv. Phys.,* 1969, **18**, 193-335.

[2] K. Rossnagel, On the Origin of Charge-Density Waves in Select Layered Transition-Metal Dichalcogenides, *J. Phys-Condens. Mat.,* 2011, **23**, 213001.

[3] B. Sipos, A.F. Kusmartseva, A. Akrap, H. Berger, L. Forró, E. Tutiš, From Mott State to Superconductivity in 1T-TaS_2. *Nat. Mater.,* 2008, **7**, 960.

[4] S. Tang, C. Zhang, D. Wong, Z. Pedramrazi, H.-Z. Tsai, C. Jia, B. Moritz, M. Claassen, H. Ryu, S. Kahn, J. Jiang, H. Yan, M. Hashimoto, D. Lu, R.G. Moore, C.-C. Hwang, C. Hwang, Z. Hussain, Y. Chen, M.M. Ugeda, Z. Liu, X. Xie, T.P. Devereaux, M.F. Crommie, S.-K. Mo, and Z.-X. Shen, Quantum Spin Hall State in Monolayer 1T-WTe_2, *Nat. Phys.,* 2017, **13**, 683.

[5] P. Sutter, J. Wang, and E. Sutter, Wrap-Around Core-Shell Heterostructures of Layered Crystals, *Adv. Mater.,* 2019, **31**, 1902166.

[6] Y. Yu, F. Yang, X.F. Lu, Y.J. Yan, Y.-H. Cho, L. Ma, X. Niu, S. Kim, Y.-W. Son, D. Feng, S. Li, S.-W. Cheong, X.H. Chen, and Y. Zhang, Gate-Tunable Phase Transitions in Thin Flakes of 1T-TaS_2, *Nat. Nanotechnol.,* 2015, **10**, 270.

[7] R. Zhao, B. Grisafe, R.K. Ghosh, K. Wang, S. Datta, and J. Robinson, Stabilizing the Commensurate Charge-Density Wave in 1-T-Tantalum Disulfide at Higher Temperature via Potassium Intercalation, *Nanoscale*, 2019, **11**, 6016-6022.

[8] M. Remskar, V. Marinkovic, A. Prodan, and Z. Skraba, Intercalation of Vacuum Deposited Silver into 1T-TaS_2 and Its Influence on Charge Density Waves, *Surf. Sci.* 1995, **324**, L367-L370.

[9] L. Stojchevska, I. Vaskivskyi, T. Mertelj, P. Kusar, D. Svetin, S. Brazovskii, D. Mihailovic, Ultrafast Switching to a Stable Hidden Quantum State in an Electronic Crystal, *Science,* 2014, **344**, 177-180.

[10] S. Vogelgesang, G. Storeck, J.G. Horstmann, T. Diekmann, M. Sivis, S. Schramm, K. Rossnagel, S. Schäfer, C. Ropers, Phase Ordering of Charge Density Waves Traced by Ultrafast Low-Energy Electron Diffraction, *Nat. Phys.,* 2017, **14**, 184.

[11] R.E. Thomson, U. Walter, E. Ganz, J. Clarke, A. Zettl, P. Rauch, and F.J. DiSalvo, Local Charge-Density-Wave Structure in 1T-TaS2 Determined by Scanning Tunneling Microscopy, *Phys. Rev. B,* 1988, **38**, 10734-10743.

[12] R. Ang, Z. Wang, C.L. Chen, J. Tang, N. Liu, Y. Liu, W.J. Lu, Y.P. Sun, T. Mori, and Y. Ikuhara, Atomistic Origin of an Ordered Superstructure Induced Superconductivity in Layered Chalcogenides, *Nat. Commun.,* 2015, **6**, 6091.

[13] J.A. Wilson, F.J. Di Salvo, and S. Mahajan, Charge-Density Waves and Superlattices in the Metallic Layered Transition Metal Dichalcogenides, *Adv. Phys.,* 1975, **24**, 117-201.

[14] T. Ritschel, J. Trinckauf, K. Koepernik, B. Büchner, M.v. Zimmermann, H. Berger, Y.I. Joe, P. Abbamonte, and J. Geck, Orbital Textures and Charge Density Waves in Transition Metal Dichalcogenides, *Nat. Phys.,* 2015, **11**, 328-331.

[15] S.M. Wu, A. Luican-Mayer, and A. Bhattacharya, Nanoscale Measurement of Nernst Effect in Two-Dimensional Charge Density Wave Material 1T-TaS_2, *Appl. Phys. Lett.,* 2017, **111**, 223109.

[16] S.-W. Hla, V. Marinković, A. Prodan, and I. Muševič, STM/AFM Investigations of β-$MoTe_2$, α-$MoTe_2$ and WTe_2, *Surf. Sci.,* 1996, **352-354**, 105-111.

[17] D. Cho, S. Cheon, K.-S. Kim, S.-H. Lee, Y.-H. Cho, S.-W. Cheong, and H.W. Yeom, Nanoscale Manipulation of the Mott Insulating State Coupled to Charge Order in 1T-TaS_2, *Nat. Commun.,* 2016, **7**, 10453.

[18] D. Cho, G. Gye, J. Lee, S.-H. Lee, L. Wang, S.-W. Cheong, and H.W. Yeom, Correlated Electronic States at Domain Walls of a Mott-Charge-Density-Wave Insulator 1T-TaS_2, *Nat. Commun.,* 2017, **8**, 392.

[19] Z. Wang, Y.-Y. Sun, I. Abdelwahab, L. Cao, W. Yu, H. Ju, J. Zhu, W. Fu, L. Chu, H. Xu, and K.P. Loh, Surface limited superconducting phase transition on 1T-TaS2, *ACS Nano*, 2018, **12**, 12619-12628.

[20] J. Skolimowski, Y. Gerasimenko, and R. Žitko, Mottness Collapse without Metallization in the Domain Wall of the Triangular-Lattice Mott Insulator 1T-TaS_2, *Phys. Rev. Lett.,* 2019, **122**, 036802.

[21] S.-W. Hla, Atom-by-Atom Assembly, *Rep. Prog. Phys.,* 2014, **77**, 056502.

[22] N.P. Guisinger, M.E. Greene, R. Basu, A. Baluch, and M.C. Hersam, Room Temperature Negative Differential Resistance through Individual Organic Molecules on Silicon Surfaces, *Nano Lett.,* 2004, **4**, 55-59.

[23] M. Grobis, A. Wachowiak, R. Yamachika, and M.F. Crommie, Tuning Negative Differential Resistance in a Molecular Film, *Appl. Phys. Lett.,* 2005, **86**, 204102.

[24] I.-W. Lyo, and P. Avouris, Negative Differential Resistance on the Atomic Scale: Implications for Atomic Scale Devices, *Science,* 1989, **245**, 1369.

[25] K.S. Kim, T.-H. Kim, A.L. Walter, T. Seyller, H.W. Yeom, E. Rotenberg, and A. Bostwick, Visualizing Atomic-Scale Negative Differential Resistance in Bilayer Graphene, *Phys. Rev. Lett.,* 2013, **110**, 036804.

[26] J.J. Kim, W. Yamaguchi, T. Hasegawa, and K. Kitazawa, Observation of Mott Localization Gap using Low Temperature Scanning Tunneling Spectroscopy in Commensurate 1T-TaS_2, *Phys. Rev. Lett.,* 1994, **73**, 2103-2106.

[27] L. Ma, C. Ye, Y. Yu, X.F. Lu, X. Niu, S. Kim, D. Feng, D. Tománek, Y.-W. Son, X.H. Chen, and Y. Zhang, A Metallic Masaic Phase and the Origin of Mott-Insulating State in 1T-TaS_2, *Nat. Commun.,* 2016, **7**, 10956.

[28] N.V. Smith, S.D. Kevan, and F.J. DiSalvo, Band Structures of the Layer Compounds 1T-TaS_2 and 2H-$TaSe_2$ in the Presence of Commensurate Charge-Density Waves, *J. Phys. C: Solid State Phys.,* 1985, **18**, 3175-3189.

[29] P. Fazekas, and E. Tosatti, Electrical, Structural and Magnetic Properties of Pure and Doped 1T-TaS_2, *Philos. Mag. B,* 1979, **39**, 229-244.

[30] L. Perfetti, P.A. Loukakos, M. Lisowski, U. Bovensiepen, M. Wolf, H. Berger, S. Biermann, and A. Georges, Femtosecond Dynamics of Electronic States in the Mott Insulator 1T-TaS_2 by Time Resolved Photoelectron Spectroscopy, *New J. Phys.,* 2008, **10**, 053019.

[31] L. Gasparov, K.G. Brown, A.C. Wint, D.B. Tanner, H. Berger, G. Margaritondo, R. Gaál, and L. Forró, Phonon Anomaly at the Charge Ordering Transition in 1T-TaS_2, *Phys. Rev. B,* 2002, **66**, 094301.

[32] X.-L. Yu, D.-Y. Liu, Y.-M. Quan, J. Wu, H.-Q. Lin, K. Chang, and L.-J. Zou, Electronic Correlation Effects and Orbital Density Wave in the Layered Compound, *Phys. Rev. B,* 2017, **96**, 125138.

[33] P. Darancet, A.J. Millis, and C.A. Marianetti, Three-Dimensional Metallic and Two-Dimensional Insulating Behavior in Octahedral Tantalum Dichalcogenides. *Phys. Rev. B,* 2014, **90**, 045134.